Constraint-based modelling captures the metabolic versatility of *Desulfovibrio vulgaris*

Jason J. Flowers,^{1†} Matthew A. Richards,² Nitin Baliga,² Birte Meyer¹ and David A. Stahl^{1*}

¹Department of Civil and Environmental Engineering, University of Washington, Seattle, WA, USA.

²Institute for Systems Biology, Seattle, WA, USA.

Summary

A refined Desulfovibrio vulgaris Hildenborough flux balance analysis (FBA) model (iJF744) was developed, incorporating 1016 reactions that include 744 genes and 951 metabolites. A draft model was first developed through automatic model reconstruction using the ModelSeed Server and then curated based on existing literature. The curated model was further refined by incorporating three recently proposed redox reactions involving the Hdr-Flx and Qmo complexes and a lactate dehydrogenase (LdhAB, DVU 3027-3028) indicated by mutation and transcript analyses to serve electron transfer reactions central to syntrophic and respiratory growth. Eight different variations of this model were evaluated by comparing model predictions to experimental data determined for four different growth conditions - three for sulfate respiration (with lactate, pyruvate or H₂/CO₂-acetate) and one for fermentation in syntrophic coculture. The final general model supports (i) a role for Hdr-Flx in the oxidation of DsrC and ferredoxin, and reduction of NAD⁺ in a flavin-based electron confurcating reaction sequence, (ii) a function of the Qmo complex in receiving electrons from the menaquinone pool and potentially from ferredoxin to reduce APS and (iii) a reduction of the soluble DsrC by LdhAB and a function of DsrC in electron transfer reactions other than sulfite reduction.

Introduction

Most biogeochemical transformations are mediated by a community of interacting organisms that together share the available free energy of a reaction sequence. In turn, the organisms that participate in the food webs that sustain major environmental processes exhibit considerable metabolic flexibility, serving for the assembly of different interaction networks in response to shifting nutrient availability. This adaptive flexibility is exemplified by the sulfate-reducing bacteria. For example, the model sulfate reducer Desulfovibrio vulgaris Hildenborough participates in the reductive steps of both the sulfur and carbon cycles, producing sulfide when growing by sulfate respiration (Voordouw, 1995) and contributing to methane production when syntrophically coupled with a hydrogenotrophic methanogen by interspecies H₂/formate transfer (Walker et al., 2009). The very different energy environments associated with these two lifestyles require a shuffling of electron transfer systems to maintain redox balance and to service energy recovery for maintenance and growth (Mever et al., 2013a). This metabolic versatility is reflected by the abundance of energy conservation associated proteins in D. vulgaris Hildenborough, many of which appear redundant, for example, the multiple periplasmic hydrogenases, membrane-bound electron-transferring complexes and electron carriers.

The complexity of the electron transfer system has complicated a fully reductionist understanding of the metabolic flexibility of D. vulgaris Hildenborough growth under different environmental conditions. Even with more recent advances in genetic methods (Fels et al., 2013; Kuehl et al., 2014) and gene expression analyses (Walker et al., 2009; Pereira et al., 2008; Meyer et al., 2013b), the model of the electron transfer system sustaining growth by sulfate respiration is still evolving (Keller and Wall, 2011; Pereira et al., 2011; Keller et al., 2014) with improved understanding of the coupling mechanisms of the different interacting redox proteins, for example, the multiple lactate dehydrogenases (Ldhs) encoded in the genome of D. vulgaris Hildenborough (Keller and Wall, 2011; Meyer et al., 2013b; Keller et al., 2014; Vita et al., 2015). Reported as membraneassociated proteins based on a study of Desulfovibrio desulfuricans, the Ldhs were initially assumed to energetically couple lactate oxidation with reduction of the menaguinone pool (Czechowski, M.H, and Rossmoore, 1990). However, a recent study reported the oligomeric LdhAB (DVU3027-3028) to contain subunits similar to the iron-sulfur subunits of heterodisulfide reductase (HdrB/HdrD), suggesting an interaction with a dithiol/ disulfide containing electron carrier rather than the menaguinone pool (Pereira et al., 2011; Meyer et al., 2013b). It was hypothesized that oxidation of lactate by LdhAB can be coupled to reduction of oxidized DsrC. the reduction of DsrC pulling the reaction (Meyer et al., 2013a,b). During syntrophic growth, reoxidation of DsrC was suggested to be mediated by a flavin-based electron confurcation involving reduced ferredoxin and the Qmo membrane complexes (Fig. 1). In contrast, during sulfidogenic growth DsrC is predicted to function by receiving electrons from three alternative membrane complexes (DsrMJKOP - DVU1286-1290, HmcABCDEF DVU0531-0536 or TmcABCD -DVU0263-0266). Reduced DsrC was recently predicted to function as a carrier of the sulfur atom originating from sulfite, generated by an initial two-electron reduction and dehydration step of sulfite by the sulfite reductase DsrAB (DVU0402-3) to form an S^{II} intermediate and second two-electron reduction step mediated by the two conserved cysteine residues of DsrC which leads to a protein-based S⁰ trisulfide (Santos et al., 2015). A subsequent four-electron reduction by the DsrMJKOP complex then releases sulfide and recycles DsrC, thereby coupling sulfite reduction to energy conservation.

Similarly, the HdrABC-FlxABCD (for heterodisulfide reductase/NADH oxidoreductase, DVU2398-2404) complex has been previously proposed to be involved in electron bi-/confurcation to partition electrons between ferredoxin, NADH, and a dithiol electron carrier (likely DsrC, DVU2776) (Meyer et al., 2013b; Pereira et al., 2011; Price et al., 2014). However, since the in vivo electropotential of DsrC is not known, it is uncertain whether the electrons from reduced ferredoxin and DsrC are confurcated into NAD+, or alternatively, reduced ferredoxin and NADH confurcate their electrons to reduce an oxidized DsrC. Although direct biochemical evidence is not available, two recent mutant studies of Desulfovibrio alaskensis G20 (Meyer et al., 2014) and D. vulgaris Hildenborough (Ramos et al., 2015) presented the first evidence for the second reaction sequence.

Lastly, previous models of sulfate reduction pathways predicted that electrons for adenosine 5'-phosphosulfate (APS) reduction were derived solely from the menaquinone pool via the quinone-interacting membrane-bound oxidoreductase (QmoABCD, DVU0848–0851), but a recent study suggested that an additional lower redox potential partner is needed in another electron confurcation process to help drive the reaction, since the redox potential difference between menaquinone oxidation (E°/MQ/MQH2 –75 mV) and APS reduction (E°/APS/SO³³ = -60 mV) is small (Ramos $et\ al.$, 2015). While these new proposed reactions were informed by protein

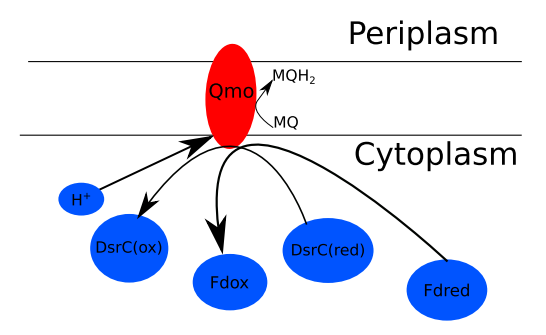


Fig. 1. Predicted Qmo complex reaction under lactate fermentation conditions. Red Circles are enzymatic proteins and blue circles represent metabolites.

structure analysis and thermodynamic considerations, none of these variants have been evaluated in the context of the associated metabolic network.

Constraint-based metabolic modelling uses the genomic content of a microbial genome to predict all central metabolic reactions of the respective microorganism. Using previously published biochemical and thermodynamic knowledge of these reactions, a stoichiometrically and charge-balanced network of reactions is constructed and constrained. Additionally, a reaction is added to account for biomass production based on the composition of the organism. Using the biomass equation, the expected growth of the organism can be predicted under various environmental growth conditions through using flux balance analysis (FBA) to find which pathway through the reaction network will maximize a cellular process. For this study, we assume the primary objective is biomass production. Since the reaction network is underdetermined, there are multiple pathways that result in the same solution. However, the resulting models can be combined with various 'omics' data for refining the expected growth which render them useful for predicting gene essentiality (Lewis et al., 2010) as well as strategies for metabolic engineering (Burgard et al., 2003).

Our previous study developed a constraint-based FBA model for D. vulgaris Hildenborough as part of a broader study that investigated its syntrophic interactions with Methanococcus maripaludis S2 (Stolvar et al., 2007). While the model was sufficient to effectively predict the interactions within the constrained conditions tested, it only contained 89 reactions, which were not linked to their associated genes. Additionally, that model did not fully capture the metabolic versatility of Desulfovibrio species, nor did it incorporate new understanding of associated electron transfer reactions. We, therefore, developed a revised, more complete constraint-based FBA model of *D. vulgaris* Hildenborough incorporating new understanding of central redox systems for the different growth modes. Several model versions, examining alternative electron transfer systems, were used to explore the importance of those systems to sulfate respiratory (lactate, pyruvate or H_2 -acetate consuming) and lactate fermentative syntrophic, growth modes. The revised model captured most features of these alterna-tive *Desulfovibrio* lifestyles and offers a framework to fur-ther refine the role of the supporting electron transfer systems.

Results and discussion

FBA model refinement

Using the recently improved annotation of the D. vulgaris Hildenborough genome (Price et al., 2011), our initial model reconstruction was auto-generated using the ModelSeed Server (Henry et al., 2010). The model was then manually curated by adding missing reactions in metabolic pathways through literature search as well as by comparing genes present to published KEGG and MetaCyc pathways and for D. vulgaris Hildenborough (Schellenberger et al., 2010; Caspi et al., 2014), and the reversibility of reactions were adjusted based on previous predictions in other organisms (Schellenberger et al., 2010). As part of the curation, reactions in the electron transfer pathway for both sulfate respiration and syntrophic fermentation included recent advances in our knowledge of electron carrier-redox protein interactions (Venceslau et al., 2010; Pereira et al., 2011; Ramos et al., 2012; Meyer et al., 2013a,b; 2014). To simplify the model, both periplasmic hydrogenases (HynAB, HydAB) were treated as a single reaction since they catalyse the same reaction. The biomass equation was based on modifying the equation from Escherichia coli model (iAF1260) (Feist et al., 2007). The resulting D. vulgaris Hildenborough model (iJF744) consisted of 1016 reactions that included 744 genes and 951 metabolites.

Model evaluation under different growth conditions

The model variants examined the recently proposed stoichiometries of electron carriers for the Qmo, Hdr-Flx and oligomeric lactate dehydrogenases, LdhABs.

Quinone-interacting membrane-bound oxidoreductase (Qmo)

$$APS+2H_{in}^{+}+MQH_{2} \rightarrow SO_{3}^{2-}+2H_{ex}^{+}+MQ+AMP$$
 (1)

$$\begin{array}{l} {\rm APS} + {}^{1}/{}_{2}{\rm Fd}_{\rm red} + 2{\rm H}_{\rm in}^{+} + {}^{1}/{}_{2}{\rm MQH_{2}} \\ \rightarrow {\rm SO_{3}^{2}} + {}^{1}/{}_{2}{\rm Fd_{ox}} + {\rm H}_{\rm ex}^{+} + {}^{1}/{}_{2}{\rm MQ} + {\rm AMP} \end{array} \tag{2}$$

Heterodisulfide reductase/NADH reductase (Hdr-Flx)

$$Fd_{red} + 2NAD^{+} + DsrC_{red} \rightarrow Fd_{ox} + 2NADH + DsrC_{ox}$$
 (3)

$$Fd_{red} + 3H^{+} + NADH + 2 DsrC_{ox}$$

$$\rightarrow Fd_{ox} + NAD^{+} + 2 DsrC_{red}$$
(4)

Lactate Dehydrogenase (Ldh)

$$Lactate + DsrC_{ox} \rightarrow Pyruvate + DsrC_{red}$$
 (5)

Lactate+MQ
$$\rightarrow$$
 Pyruvate+MQH₂ (6)

where:

APS = adenosine-5-phosphosulfate

AMP = adenosine monophosphate

MQ = menaquinone

MQH₂ =menaquinol

 $Fd_{red} = reduced ferredoxin$

Fd_{ox} = oxidized ferredoxin

NAD⁺ = oxidized nicotinamide adenine dinucleotide

NADH = reduced nicotinamide adenine dinucleotide

 $DsrC_{red} = reduced$ dissimilatory sulfite reductase C protein

 $DsrC_{ox} = oxidized$ dissimilatory sulfite reductase C protein

 $H^+ = proton$

To assess which stochiometric reaction variants best reflect the physiological data, we developed eight different versions of the model using CobraToolbox in MATLAB and simulated growth under four different growth conditions (lactate- and pyruvate-limited sulfate respiration, hydrogen-limited sulfate respiration, and lactate fermentation which is the best representation of syntrophic growth) by changing the exchange fluxes in the model. The two model variants for Ldh were only investigated for growth on lactate (lactate-limited sulfate respiration and lactate fermentation).

For flux simulations under all growth conditions, the expected growth rate was set to 0.06 h⁻¹ by constraining the electron donor uptake rate to meet that growth rate based on previous experimental data (Badziong and Thauer, 1978; Traore et al., 1983; Villanueva et al., 2008). Because the GAM and NGAM vary among the growth conditions, the GAM and NGAM were determined as previously outlined in the Materials and Methods Section. Table 1 shows the results for the predicted growth rate and electron donor to electron acceptor flux ratios under each condition for all model variants. Models 4, 5, 6 and 8 were not able to match the expected growth rate under lactate-sulfate growth conditions (Table 1). In addition, not all of the remaining model variants were able to accurately predict electron donor to electron acceptor ratios for every growth condition. For instance, under hydrogen-sulfate growth conditions, Model 3 did not produce accurate hydrogen to sulfate flux ratio predictions (2775:1 model vs. 4:1 theoretical) as shown on Table 1. Therefore, any other flux results from this model variant could not be expected to

rable 1. Estimated growth rate and flux ratios for multiple model variants of the QMO, Hdr-Flx and Ldh reactions under four different growth conditions

Qmo HdrFlox	HdrFlox	,Flox		٦	- l		Lacate sulfate	sulfate	Pyruvate sulfate	sulfate	Hydroge	Hydrogen sulfate	Lactate fermentation (simulated co-culture)	nentation to-culture)
Expected growth Eq. 2 Eq. 3 Eq. 4 Eq. 5 Eq. 6 rate, hr ⁻¹	Eq. 5 Eq. 6 r	Eq. 5 Eq. 6 r	5 Eq. 6 r	9 6	Expected growth rate, hr ⁻¹		Simulated growth rate, hr ⁻¹	Lacate/ sulfate flux ratio	Simulated growth rate, hr ⁻¹	Pyruvate/ sulfate flux ratio	Simulated growth rate, hr ⁻¹	Hydrogen/ Sulfate Flux Ratio	Simulated growth rate, hr ⁻¹	Lactate/ acetate flux ratio
90.00 × ×	0.00 × ×	90.00 ×	90.0 X	90.0	90.0	1	90.0	2.68	090.0	4.61	0.065	5.23	×	×
90.00 × × ×	90.0 ×	90.0 ×	90:00 ×	90.0	90.0		90.0	2.68	0.059	4.58	090.0	5.21	0.060	1.519
90.0 × ×	90.0 × ×	90.0 × ×	90:00 ×	90:0	90.0		90.0	2.68	090.0	380.79	090.0	2775.72	×	×
90.0 × × ×	90.0 × ×	90.0 × ×	90:00 X	90.0	90.0		0.129	2.93	090.0	380.79	090.0	2775.72	090.0	1.505
90:0 X X	0.00 X	90:0 X	90:00 X	90.00 X	90.0		0.028	4.33	×	×	×	×	×	×
90:0 X X X	0.00 X X	90:0 X	0.00 ×	90:00 X	90.0		0.162	3.07	×	×	×	×	90.0	1.896
90.00 X X	90.0 X X	90:00 ×	90.0 ×	90:00 X	90.0		0.063	2.69	×	×	×	×	×	×
90:0 × ×	90:0 X X	90:00 ×	90:00 ×	90:00 X	90.0		0.876	56.63	×	×	×	×	90.0	1.505

accurately predict growth. As a result, model 3 was no longer considered. For lactate-sulfate growth, the stochiometric molar ratio of lactate oxidized to sulfate reduced is \sim 2. However the predicted lactate:sulfate ratio from Model 8 was significantly higher (58:1). Therefore, Model 8 was not further evaluated. Similarly, Models 5 and 6 were also discarded because both predicted lactate:sulfate ratios (4.33 and 3.07 respectively) higher than the expected stochiometric molar ratio. Models 1 and 2, which only differed in Qmo reactions (Eqs. (1) and (2)), predicted the flux ratios for lactate-sulfate closest to the expected ratio under lactate-sulfate conditions Therefore, either Qmo reaction variant appears to be feasible, but considering the thermodynamic and experimental evidence for the ferredoxin and menaguinone coupling confurcation reaction driving APS reduction (Ramos et al., 2012), the Eq. (2) variant (Model 2) is deemed most likely. Based on this analysis, Eq. (5) variant of Ldh, coupling lactate oxidation to reduction of oxidized DsrC rather than the menaquinol pool, and the Eq. (3) variant of Hdr-Flx, in which NAD⁺ is reduced by DsrC and ferredoxin, are considered the most feasible variants. Therefore, Model 2 is most consistent with the physiological data for D. vulgaris Hildenborough for the four simulated growth conditions investigated in this work. The reconstructed network model (iJF744) is provided in the Supporting Information in SBML format.

Evaluation of model predictions

Since FBA is mathematically under-determined, which means that the solution is not set and each reaction can have a range of fluxes to meet the objective of maximizing growth rate, FVA was performed using the Cobra Toolbox. FVA determined the range of fluxes that reactions can have while maintaining the optimal growth rate, essentially defining the flexibility of each reaction. Therefore, FVA is advantageous over FBA because it helps to define the flux bounds for each reaction under the tested growth conditions. In addition, FVA can also identify reactions with less certain roles by finding reactions with flux ranges that encompass zero. To understand some of the potential metabolic pathways used for growth under different growth conditions, FVA was performed on the model under lactate-limited sulfate respiration (lactate-sulfate), pyruvate-limited sulfate respiration (pyruvate-sulfate), hydrogen-limited sulfate respiration (hydrogen-sulfate) and lactate fermentation growth conditions.

Lactate-sulfate growth. For growth on lactate-sulfate media, the overall expected stoichiometry is:

2 Lactate+
$$SO_4^{2-} \rightarrow 2$$
 Acetate+ H_2S+2 HCO $_3^-$ (7)

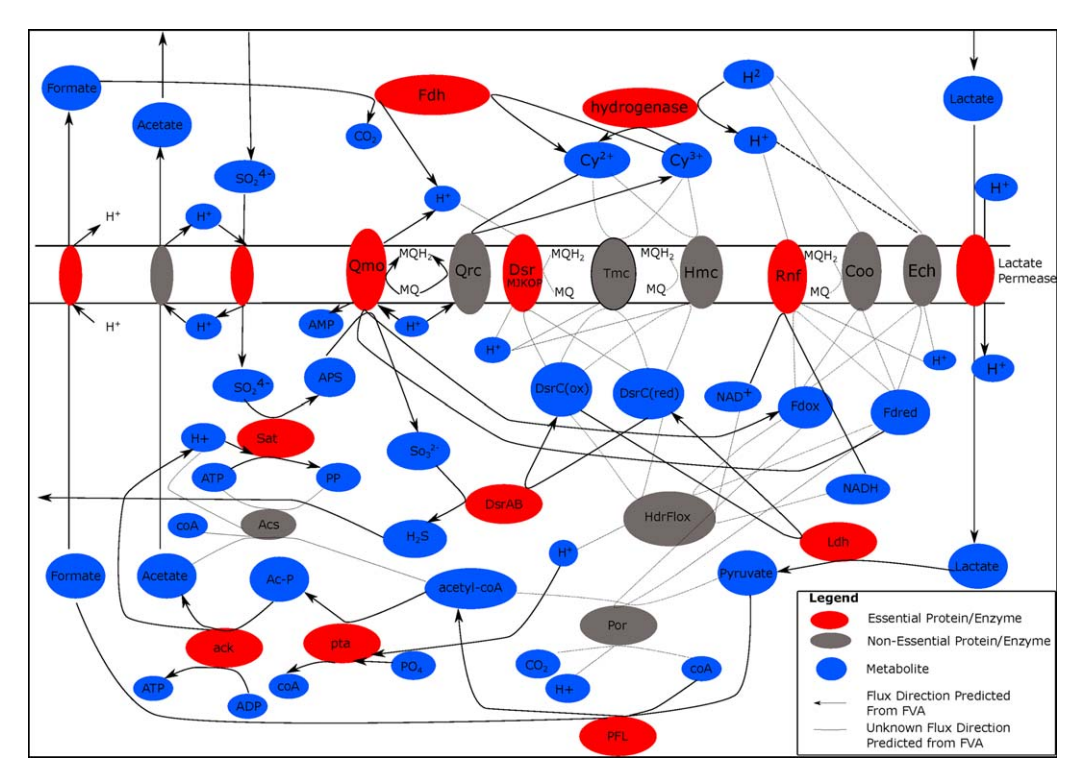


Fig. 2. Predicted flux distributions of key metabolic reactions for ijf744 model under lactate sulfate growth conditions. Red and grey circles are enzymatic proteins and blue circles represent metabolites. Red circles are enzymatic proteins that were found to be essential under the growth condition (growth ration < 0.8). Lines with black arrows show reaction direction predicted by FVA analysis. Dashed lines show reactions for which direction is not determined by FVA.

To model growth under these conditions, sulfate flux was unconstrained and the lactate flux was constrained to provide enough electron donor to support a 0.06 day⁻¹ growth rate. To simplify and visualize the results of the FVA analysis, Fig. 1 shows the direction of flux predicted for several key reactions associated with energy generation. If the minimum and maximum fluxes are in the same direction, the reaction flux arrow shows the predicted direction in black. If the direction of metabolic flux through a reaction is not certain because the minimum and maximim fluxes in the FVA are in opposite directions, then the flux reaction arrow is removed and the flux represented by a dashed line. Blue circles represent metabolites. Red circles are enzymatic proteins that were found to be essential under the growth condition (growth ration < 0.8). Grey circles are enzymatic reactions found to be non-essential. If no flux is predicted in the FVA, then the arrow and reaction is not graphed. As shown in Fig. 2, the model predicted a rather extensive network of electron transfer proteins contributing to growth. Lactate oxidation to acetate is mediated by Ldh and pyruvate-formate lyase (Pfl, DVU2824-25) to form formate and acetyl-CoA with the latter being used to produce ATP through substratelevel phosphorylation by phosphotransacetylase (Pta,

DVU3029) and acetate kinase (Ack, DVU3030). Overall, the model shows a near 1:1 flux ratio of acetate excretion to lactate utilization as expected. Previous reports have suggested that pyruvate ferredoxin oxidoreductase (PorAB, DVU1569, DVU1570) to acetyl-CoA is the primary route of pyruvate oxidation. FVA does show that growth is possible using PorAB enzyme, but the FVA does not clearly resolve direction or contribution of PorAB to growth.

Interestingly, as shown on Fig. 1, the formate produced is predicted to be exported to the periplasm where it is oxidized by a formate dehydrogenase (Fdh, DVU0587-8, DVU2809–2812 and DVU2481–2485), generating proton motive force and reduced periplasmic type-I cytochrome c_3 . This is in agreement with previous research showing growth inhibition on lactate-sulfate growth media for Δ Fdh mutants, suggesting that formate cycling is important for respiratory growth (Caspi *et al.*, 2014; da Silva 2013). The reduced type-I cytochrome c_3 subsequently interacts with the quinone-reducing complex (Qrc, DVU 0692–0695) to reduce the menaquinone pool.

Previous research suggested hydrogen cycling to be an essential general mechanism of energy coupling for respiratory growth in *Desulfovibrio* species (Odom and Peck, 1981). Our model also predicts the involvement of

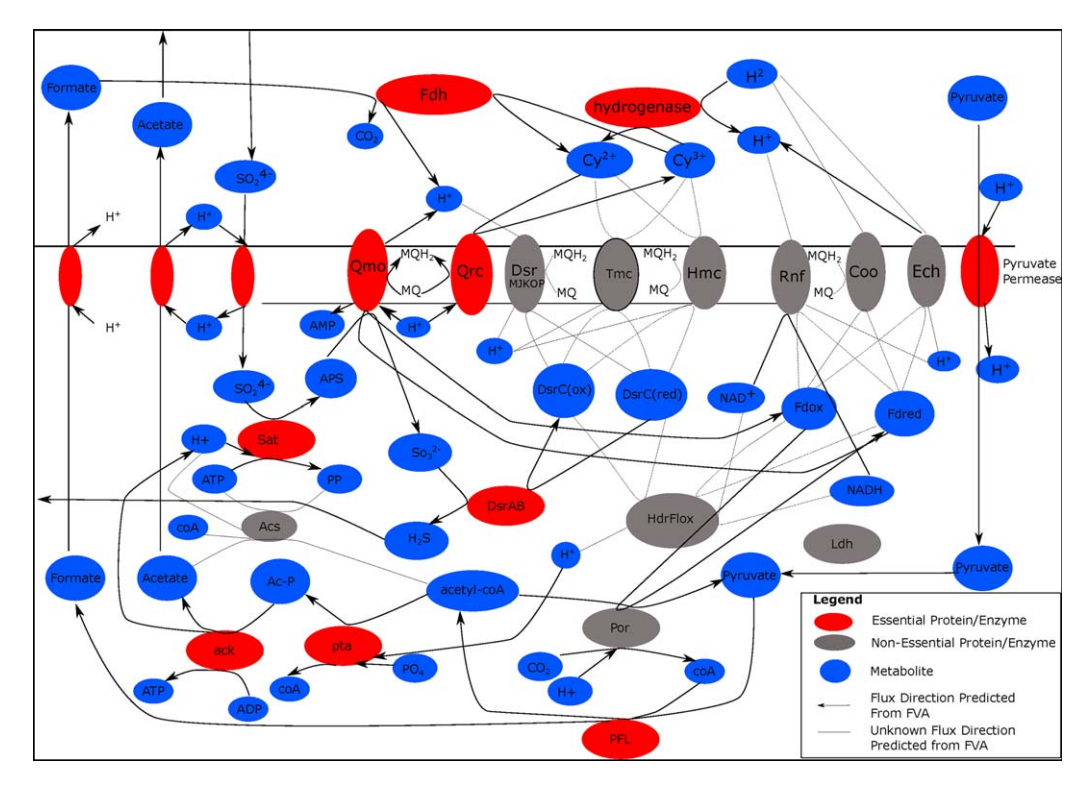


Fig. 3. Predicted flux distributions of key metabolic reactions for ijf744 model under pyruvate sulfate growth conditions. Red and grey circles are enzymatic proteins and blue circles represent metabolites. Red circles are enzymatic proteins that were found to be essential under the growth condition (growth ration < 0.8). Lines with black arrows show reaction direction predicted by FVA analysis. Dashed lines show reactions for which direction is not determined by FVA.

hydrogen cycling by flux through periplasmic hydrogenases; however, the source of hydrogen is not determined since the potential involvement of several membrane-bound hydrogenases including Ech hydrogenase (DVU 0429–0434), Coo hydrogenase (DVU 2286–2291) and the Rnf complex (DVU 2791–2797) is not certain. Notably, a previous study showed that deletion of the Coo hydrogenase genes has no impact on sulfate respiratory growth on lactate (Walker *et al.*, 2009). Consistent with those experimental data, no growth rate deficit on lactate-sulfate was observed when this hydrogenase was removed from the model.

Pyruvate-sulfate growth. For pyruvate-sulfate growth media, the standard stoichiometry is:

4 Pyruvate+
$$SO_4^{2-}$$
+4 $H_2O \rightarrow$ 4 Acetate + H_2S +4 HCO_3^- +2 H^+

Similar to lactate-sulfate growth conditions, Fig. 3 shows the direction of flux predicted by FVA for several key reactions associated with energy generation under pyruvate-sulfate growth conditions. Similar to lactate-sulfate growth, pyruvate is predicted to be oxidized by the pyruvate-formate lyase, and the resulting acetyl-CoA then used for substrate-level phosphorylation to produce acetate through Pta and Ack (see Fig. 3). The FVA

results also suggest that some of the pyruvate is oxidized by POR to acetyl-CoA. The formate produced from pyruvate-formate lyase is exported to the periplasm where it is oxidized by the

Fdh. Flux through a periplasmic hydrogenase is also predicted, but the source of hydrogen is unknown since the flux through Ech, Coo and Rnf is not determined. Although the flux for Hdr-Flx is not determined under pyruvate-based sulfate respiration in this model, previous studies showed that growth of Hdr-Flx insertion mutants of *Desulfovibrio alaskensis* G20 were impaired relative to the wild type (Meyer *et al.*, 2014).

Hydrogen-sulfate growth. For growth on a hydrogen/CO₂-acetate-sulfate medium, the overall expected stoichiometry is:

$$4\ H_2 + SO_4^{2-} \to H_2S + 2\ H_2O + 2\ OH^-$$

As expected, the flux distribution for hydrogen-sulfate growth is quite different than lactate- and pyruvate-sulfate growth conditions (see Fig. 4). With hydrogen serving as the source of electrons for growth, both the periplasmic hydrogenases and the membrane-bound hydrogenase Ech are predicted to oxidize hydrogen to reduce type-I cytochrome c_3 and ferredoxin respectively.

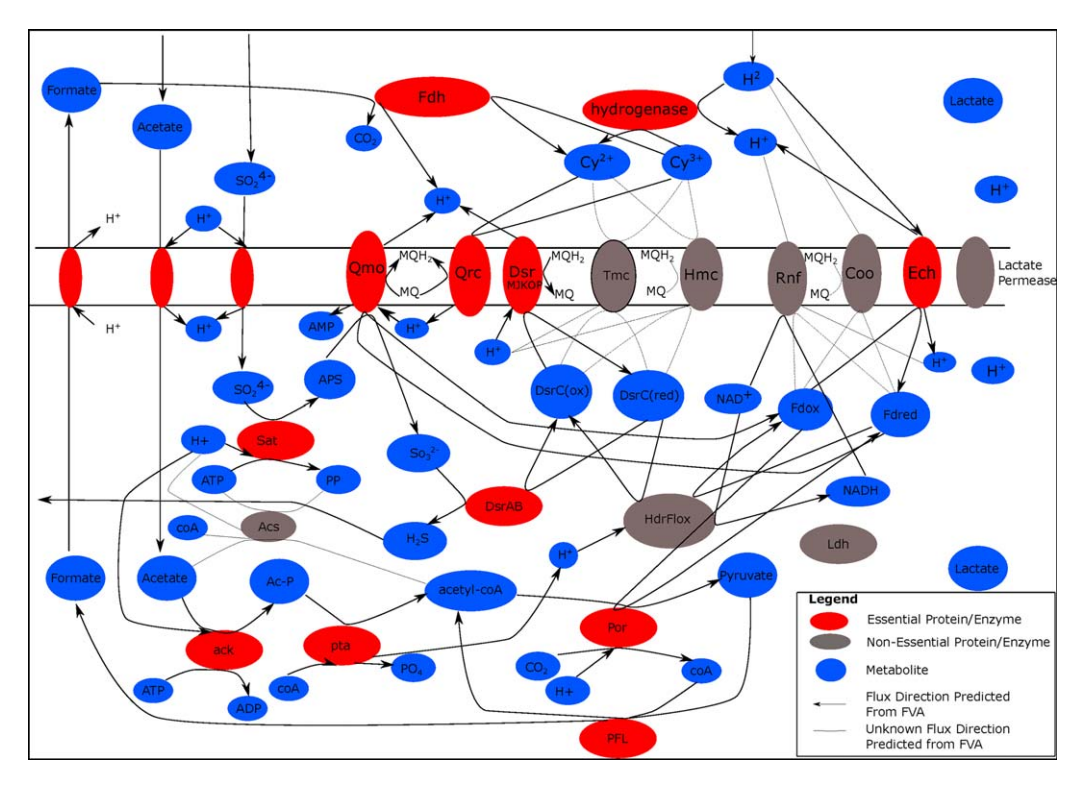


Fig. 4. Predicted flux distributions of key metabolic reactions for ijf744 model under hydrogen sulfate growth conditions. Red and grey circles are enzymatic proteins and blue circles represent metabolites. Red circles are enzymatic proteins that were found to be essential under the growth condition (growth ration < 0.8). Lines with black arrows show reaction direction predicted by FVA analysis. Dashed lines show reactions for which direction is not determined by FVA.

The reduced ferredoxin is predicted to reduce acetate to pyruvate via POR for anaplerotic reactions and for NADH production and APS reduction via the Hdr-Flx and Qmo complexes respectively. The reduced type-I cytochrome c3 is mostly used to reduce the menaquinone pool through Qrc, which is either used to reduce APS through Qmo or to reduce DsrC for sulfite reduction. Interestingly, the model predicts some of the pyruvate to be transformed to formate (via Pfl) which is then oxidized by Fdh in the periplasm to produce reduced type-I cytochrome c₃ (similar to lactate-sulfate and pyruvate-sulfate growth). No evidence was found in the existing literature for this reaction sequence, but removing the formate dehydrogenase reaction from the model made growth infeasible. Thus, the model provides a clear framework for experimental validation.

Lactate fermentation. For fermentative growth on a lactate medium, the overall expected stoichiometry is:

$$Lactate + H_2O \rightarrow Acetate + 2 \ H_2 + CO_2$$

Sustained growth by lactate fermentation under standard conditions is infeasible for *D. vulgaris* Hildenborough due to its low thermodynamic yield (ΔG^{0} , = -8.8 kJ/mole) (Walker *et al.*, 2009). Growth ceases when the fermentation products including H₂ and acetate accumulate in the

growth media (Walker et al., 2009; Meyer et al., 2013b). However, in syntrophic association with a hydrogenotrophic methanogen, the thermodynamic yield increases significantly ($\Delta G \approx -67.3$ kJ/mole) and growth is sustained by continuous consumption of the fermentative products by the methanogen (Walker et al., 2009). To understand the likely metabolic pathways used under these conditions, the model simulated syntrophic growth by providing an external sink for acetate, carbon dioxide and hydrogen to simulate uptake by methanogens. To be consistent with the other simulated growth media, a lactate uptake rate was chosen based on the previously published growth parameters (Traore et al., 1983) to achieve a 0.06 h⁻¹ growth rate, but fermentative growth typically does not achieve the same growth rate as sulfate respiration due to the lower thermodynamic yield. Figure 5 shows the predicted flux distribution based on FVA under these conditions. After uptake, lactate is oxidized to acetate via sequential conversions by Ldh, Pfl, Pta and Ack. Some of the lactate might be oxidized to acetyl-CoA via Por, but the results of the FVA were not conclusive. The exact route of electrons yielded by Ldh to reduce DsrC is not determined, but the FVA results predict that the electrons derived from reduced DsrC could potentially be used by Tmc or Hmc to reduce periplasmic type-I cytochrome c₃ or Hdr-Flx to reduce

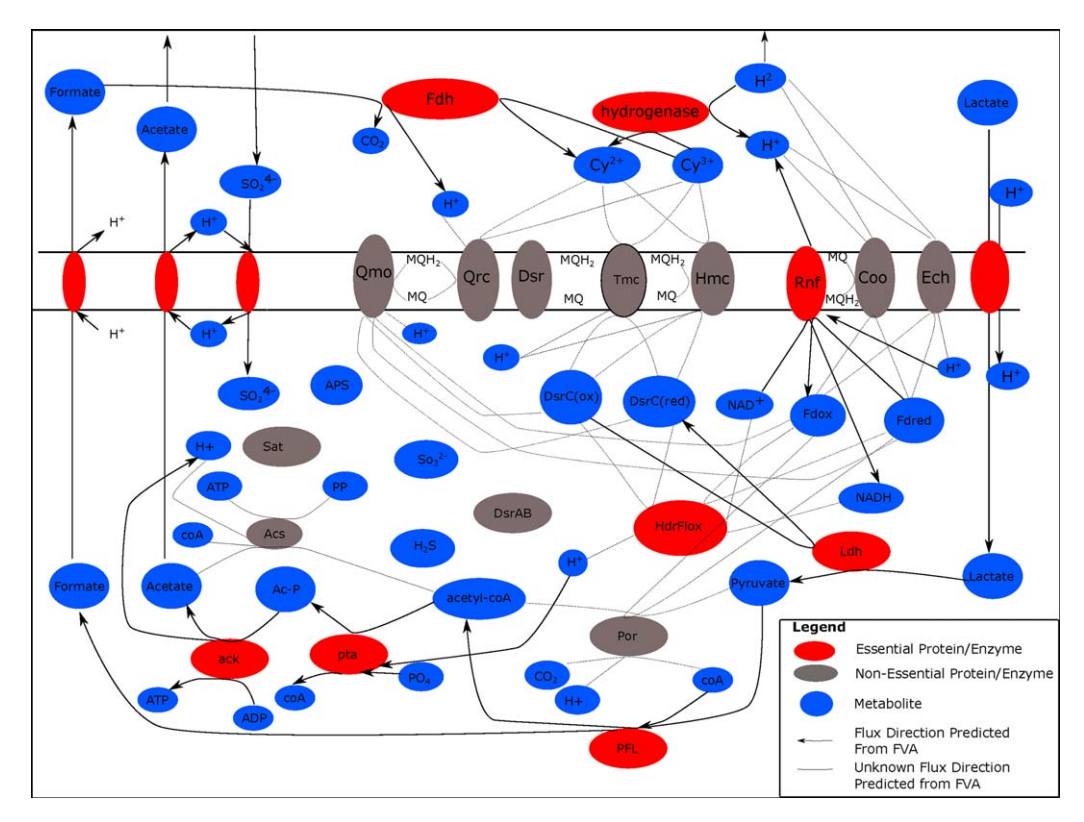


Fig. 5. Predicted flux distributions of key metabolic reactions for ijf744 model under lactate fermentation (coculture) growth conditions. Red and grey circles are enzymatic proteins and blue circles represent metabolites. Red circles are enzymatic proteins that were found to be essential under the growth condition (growth ration < 0.8). Lines with black arrows show reaction direction predicted by FVA analysis. Dashed lines show reactions which direction is not determined by FVA.

NAD⁺ to NADH. Although the model does suggest that Rnf is active in reduction of NAD⁺ to NADH, our previous studies showed that under syntrophic growth conditions there was no up-regulation of the Rnf complex (Walker *et al.*, 2009; Meyer *et al.*, 2013b). Lastly, the model results suggest that formate dehydrogenase and periplasmic hydrogenase are active under coculture conditions, which generates a proton gradient for ATP synthesis.

Essential reaction analysis

To confirm the results of the FVA analysis, a reaction essentiality analysis was performed. As part of the analysis, a series of FBA analyses were run on the model for each growth condition where a single reactions flux is set to zero, and the resulting impact on the objective function (e.g., maximizing growth rate) is determined. This was performed on the subset of reactions shown on Figs. 2–5 that include central metabolism, sulfate reduction, and electron carrier reactions. For this analysis, a growth ratio of 1.0 means that the absence of tested reaction does not impact the growth rate while a value of 0.0 means that the FBA predicts zero growth when the reaction is absent. Reactions that were either

determined to reduce the predicted growth rate by 20% or more (growth ratio < 0.8) or the simulation timed out in MATLAB, which suggests that a solution could not be determined, were assumed to be essential and are shown in red on Figs. 2–5. The results are summarized on Supporting Information Table S4.

Not surprisingly, the absence of most sulfate reduction genes (Qmo, Sat or DsrAB) prevented growth under sulfate reducing conditions (LS, PS and HS). However, absence of Qrc and DsrMJKOP did not prevent growth under some of the tested conditions. Specifically, the model showed no growth limitation for a DsrMJKOP deletion under PS conditions. Thus, its function in reducing DsrC (or a DsrC trisulfide) for sulfite reduction appeared to be compensated for by the activity of Hdr-Flx. With deletion of Qrc, growth under LS conditions was slightly impaired (growth ratio = 0.93), but significantly impacted (growth ratio < 0.5) under PS and HS conditions.

Interestingly, deletion of one of three membrane bound electron carriers (Coo, Hmc or Tmc) did not have a significant impact on growth. This lack of impact is consistent with the variable distribution of these membrane-bound electron-transferring redox complexes among sulfate reducing organisms, suggesting their

variable involvement in processes peripheral to central metabolism (Meyer et al., 2013b; Pereira et al., 2011). In contrast, deletion of two other membraneassociated complexes, Rnf and Ech, impaired growth under some conditions. Deletion of Rnf. depressed growth under coculture and LS conditions (growth ratio of 0.78 and 0.28 respectively) and Ech was firmly predicted to be actively involved only under hydrogen-sulfate conditions based on the simulation unable to find a solution when Ech was deleted from the model. Lastly, for carbon metabolism, the essential reaction analysis supports the central role of formate under sulfate reducing conditions. Deletion of Pfl results is a significant drop in predicted growth rate (growth ratio < 0.55) for all four conditions tested. This is supported by a similar impact of Fdh deletion on arowth.

Experimental procedures

Constraint-based flux balance analysis

Constraint-based FBA uses linear programming to predict the steady state conditions in metabolic systems. Using a $m \times n$ stoichiometric matrix, S, that is constructed from m metabolites and n reactions, a solution to the flux vector is found under the following equations.

$$S * v = \mathbf{0}$$
$$\alpha \le v \le \beta$$

Here, 'v' represents the vector of steady-state reaction fluxes; α and β represent the lower and upper bounds respectively, set on the fluxes. Where information is available, reaction direction and reversibility in the network are constrained based on thermodynamic predictions. For this model, thermodynamic constraints were determined by investigating the published reaction directionality based on the BIGG Database (Schellenberger et al., 2010). Additionally, reaction fluxes were subjected to two additional constraints. First, we minimized the squared sum of fluxes to restrict fluxes to more realistic values using the following equation.

$$\mathsf{Minimize} \sum_{i}^{m} v_{i}^{\mathbf{2}}$$

Furthermore, we disallowed thermodynamically infeasible flux loops in our simulations as described previously (Schellenberger *et al.*, 2011a). For the optimization, simulations were performed using the Cobra Toolbox in MATLAB (The MathWorks, Natick, MA) (Schellenberger *et al.*, 2011b). Results of the optimizations were visualized using the Paint4Net (Kostromins and Stalidzans, 2012).

Desulfovibrio vulgaris *Hildenborough model* reconstruction

Using the genome annotation from MicrobesOnline (Dehal *et al.*, 2010), which contains the recent evidence-based annotations for *D. vulgaris* Hildenborough (Price *et al.*, 2011), an initial stoichiometric matrix was automatically generated using the ModelSeed Server (Henry *et al.*, 2010). The model was exported from ModelSeed into Systems Biology Markup Language (SBML) format. The model was then curated within the Cobra toolbox in MATLAB (Schellenberger *et al.*, 2011b) by comparing reactions in the automatically-generated model against the KEGG Database (Kanehisa and Goto, 2000), Meta-Cyc (Caspi *et al.*, 2014) and the BIGG Database (Schellenberger *et al.*, 2010).

Missing reactions and metabolites were added using ModelSeed naming convention, and the reactions were added to the model using the Cobra Toolbox function addReaction addMetabolite respectively, in MATLAB. With the exception of reactions associated with energy metabolism (e.g., hydrogenases, sulfate reduction pathway and pyruvate metabolism), the reactions direction and Gene-Production-Reaction designation (GPR) produced from ModelSeed assignment were assumed to be accurate. For central energy metabolism reactions, the GPR were determined based on comparing current literature (Villanueva et al., 2008; Keller and Wall, 2011; Pereira et al., 2011; Ramos et al., 2012; 2015; Meyer et al., 2013a,b; 2014), and reactions were left reversible to allow for the model to predict directionality.

As discussed in the following section, there are several reactions that the stoichiometry was not settled in the current literature as discussed in the results section. To evaluate the different stochiometric reaction variants, two different versions of these reactions were added to the model (e.g., rxn14404A or rxn14404B) using the addReaction function in CobraToolbox, and each reactions variants were assessed by constraining the flux through one of the reaction variants to zero using the changeRxnBounds function to not allow flux through the reaction. The other stochiometric variant was not constrained to zero flux and the model was then analysed using FBA or flux variability analysis (FVA) using either optimizeCbModel or fluxVariability function respectively. Since there were three different reactions which had stochiometric reaction variants, eight different model variants were constructed and evaluated.

Construction of the biomass reaction and cell maintenance

To model the production of new cells and the demand on biosynthetic precursors, a biomass reaction was created that contained sinks for macromolecule precursors. The composition of the cell was assumed to be the same as *Escherichia coli*: 21.3% RNA, 3.23% DNA, 9.47% phospholipid, 2.6% peptidoglycan, 3.54% LPS, 57.23%, protein and 2.6% carbohydrates (Neidhardt, 1987). The biomass equation from model iAF1260 for *Escherichia coli* was modified to match the metabolite designations that were used in the automatic reconstruction of iJF744 model by changing each metabolite in the iAF1260 to match its corresponding metabolite name in the iJF744 model.

Determination of the growth and non-growth associated maintenance terms

To calculate the amount of energy that is used for nongrowth associated maintenance (NGAM), we used previously published chemostat data from multiple studies for each of the growth media conditions modelled (Badziong and Thauer, 1978; Traore et al., 1983; Villanueva et al., 2008). Using the data for each growth condition, the model objective was changed to maximize ATP hydrolysis, and the substrate uptake rates and biomass were constrained to the measured values. The predicted ATP fluxes were plotted against the growth rates to obtain the non-growth associated maintenance (NGAM; y-intercept) and the growth associated maintenance (GAM; slope) for that particular growth condition. The calculated NGAM and GAM values for each condition are shown on Supporting Information Table S2. Our scripts for determining the condition-specific maintenance parameters are available on GitHub (https://github.com/marichards/Dvh_ Model). The media formulation used for the model is included in Supporting Information Table S1.

Model and script availability

Simulating steady state growth under different conditions required changes to the model constraints that govern which pathways may carry flux. For this model, growth conditions were simulated under lactate- and pyruvatelimited sulfate respiration (LS and PS respectively), hydrogen-limited sulfate respiration (HS), and lactate fermentation, which is the best representation of syntrophic growth (CC). To assist in building these media-specific models and predicting growth, we created a set of MAT-LAB scripts that: (i) alter media conditions and internal reaction bounds to ensure the correct conditions, including modifying the GAM/NGAM values; (ii) simulate FBA or FVA to predict a steady state flux distribution; (iii) return a small set of relevant reaction fluxes in central metabolism; (iv) optionally create a map of flux in of this central subnetwork in .svg format. Our full set of scripts as well as the MATLAB and SBML versions of iJF744 are publically available at https://github.com/marichards/Dvh_ Model. Additionally, our SBML model (growing on HS media by default) is available via the Biomodels database with the identifier MODEL1706150001 (Li *et al.*, 2010).

Conclusions

A major objective of model construction was to evaluate the contribution of recently proposed redox reactions to the metabolic versatility of *Desulfovibrio* species. A fully curated *D. vulgaris* Hildenborough model was built upon an initial draft (Henry *et al.*, 2010) and updated based on recent literature (Walker *et al.*, 2009; Venceslau *et al.*, 2010; Keller and Wall, 2011; Pereira *et al.*, 2011; Meyer *et al.*, 2013a,b; Ramos *et al.*, 2015). In addition to expanding the set of reactions in central metabolism, model development and validation evaluated the recently proposed interactions and energy conserving mechanisms of three redox proteins/complexes and electron carriers of so far uncertain stoichiometry and linkage to the cellular metabolic network.

By stimulating growth under different respiratory and syntrophic conditions, we were able to evaluate alternative activities for the enzyme participating in those redox reactions, and, thereby, arrive at one general model. This expanded constraint-based FBA model (iJF744). which contains 1016 reactions including 744 genes and 951 metabolites, captured the capacity of D. vulgaris Hildenborough to grow under four distinct environmental conditions. The metabolic versatility of D. vulgaris could be attributed in part to the incorporation of multiple redox reactions. The model also supports an earlier suggestion that electron confurcation between ferredoxin and the menaquinone pool is used by the Qmo complex to reduce APS under sulfate respiration conditions (Ramos et al., 2010). Lastly, the model supports the predicted Hdr-Flx reaction that reduces NAD+ to NADH by an electron confurcation of electrons originating from ferredoxin and DsrC (Meyer et al., 2013b; Meyer et al., 2014; Ramos et al., 2015).

Although the model developed by ModelSeed was a useful initial construction, it did not incorporate the wide variety of electron carriers present in sulfate-reducing bacteria (Pereira et al., 2011) or account for the metabolic versatility of Desulfovibrio vulgaris Hildenborough. Our development of a more plausible constraint-based model required the incorporation of additional electron transfers informed by recent genetic, molecular and expression analyses. Notably, our study revealed that most of the electron carriers are not required for growth under all conditions, but rather are environment dependent. Thus, the development of the iJF744 model now offers a framework, and testable reaction mechanisms, to better understand the physiological versatility of D. vulgaris Hildenborough and other sulfate reducing bacteria.

Acknowledgements

This work conducted by Ecosystems and Networks Integrated with Genes and Molecular Assemblies (ENIGMA; http://enigma.lbl.gov), a Scientific Focus Area Program at Lawrence Berkeley National Laboratory, was supported by the Office of Science, Office of Biological and Environmental Research of the U. S. Department of Energy under Contract No. DE-AC02–05CH11231. The authors confirm the originality of the study and have no conflict of interest to declare.

References

Badziong, W., and Thauer, R.K. (1978) Growth yields and

- growth rates of Desulfovibrio vulgaris (Marburg) growing on hydrogen plus sulfate and hydrogen plus thiosulfate as the sole energy sources. *Arch Microbiol* **117**: 209–214.
- Burgard, A.P., Pharkya, P., and Maranas, C.D. (2003) Opt-knock: a bilevel programming framework for identifying gene knockout strategies for microbial strain optimization. *Biotechnol Bioeng* 84: 647–657.
- Caspi, R., Altman, T., Billington, R., Dreher, K., Foerster, H., Fulcher, C.A., et al. (2014) The MetaCyc database of metabolic pathways and enzymes and the BioCyc collection of Pathway/Genome Databases. Nucleic Acids Res 42: D459–D471.
- Czechowski, M.H., and Rossmoore, H.W. (1990) Purification and partial characterization of ad(-)-lactate dehydrogenase fromDesulfovibrio desulfuricans (ATCC 7757). *J Ind Microbiol* **6**: 117–122.
- da Silva, S.M., Voordouw, J., Leitão, C., Martins, M., Voordouw, G., and Pereira, I.A.C. (2013) Function of formate dehydrogenases in Desulfovibrio vulgaris Hildenborough energy metabolism. *Microbiol Read Engl* 159: 1760–1769.
- Dehal, P.S., Joachimiak, M.P., Price, M.N., Bates, J.T., Baumohl, J.K., Chivian, D., et al. (2010) MicrobesOnline: an integrated portal for comparative and functional genomics. *Nucleic Acids Res* 38: D396–D400.
- Feist, A.M., Henry, C.S., Reed, J.L., Krummenacker, M., Joyce, A.R., Karp, P.D., et al. (2007) A genome-scale metabolic reconstruction for Escherichia coli K-12 MG1655 that accounts for 1260 ORFs and thermodynamic information. Mol Syst Biol 3: 121.
- Fels, S.R., Zane, G.M., Blake, S.M., and Wall, J.D. (2013) Rapid transposon liquid enrichment sequencing (TnLE-seq) for gene fitness evaluation in underdeveloped bacterial systems. *Appl Environ Microbiol* 79: 7510–7517.
- Henry, C.S., DeJongh, M., Best, A.A., Frybarger, P.M., Linsay, B., and Stevens, R.L. (2010) High-throughput generation, optimization and analysis of genome-scale metabolic models. *Nat Biotechnol* 28: 977–982.
- Kanehisa, M., and Goto, S. (2000) KEGG: Kyoto encyclopedia of genes and genomes. *Nucleic Acids Res* 28: 27–30.
- Keller, K.L., and Wall, J.D. (2011) Genetics and molecular biology of the electron flow for sulfate respiration in desulfovibrio. Front Microbiol 2: 135.
- Keller, K.L., Rapp-Giles, B.J., Semkiw, E.S., Porat, I., Brown, S.D., and Wall, J.D. (2014) New model for

- electron flow for sulfate reduction in Desulfovibrio alaskensis G20. *Appl Environ Microbiol* **80**: 855–868.
- Kostromins, A., and Stalidzans, E. (2012) Paint4Net: COBRA toolbox extension for visualization of stoichiometric models of metabolism. *Biosystems* 109: 233–239.
- Kuehl, J.V., Price, M.N., Ray, J., Wetmore, K.M., Esquivel, Z., Kazakov, A.E., et al. (2014) Functional genomics with a comprehensive library of transposon mutants for the sulfate-reducing bacterium Desulfovibrio alaskensis G20. mBio 5: e01041–e01014.
- Lewis, N.E., Hixson, K.K., Conrad, T.M., Lerman, J.A., Charusanti, P., Polpitiya, A.D., *et al.* (2010) Omic data from evolved *E. coli* are consistent with computed optimal growth from genome-scale models. *Mol Syst Biol* **6**: 390.
- Li, C., Donizelli, M., Rodriguez, N., Dharuri, H., Endler, L., Chelliah, V., *et al.* (2010) BioModels database: an enhanced, curated and annotated resource for published quantitative kinetic models. *BMC Syst Biol* **4**: 92.
- Meyer, B., Kuehl, J.V., Deutschbauer, A.M., Arkin, A.P., and Stahl, D.A. (2013a) Flexibility of syntrophic enzyme systems in Desulfovibrio species ensures their adaptation capability to environmental changes. *J Bacteriol* 195: 4900–4914.
- Meyer, B., Kuehl, J., Deutschbauer, A.M., Price, M.N., Arkin, A.P., and Stahl, D.A. (2013b) Variation among Desulfovibrio species in electron transfer systems used for syntrophic growth. *J Bacteriol* **195**: 990–1004.
- Meyer, B., Kuehl, J.V., Price, M.N., Ray, J., Deutschbauer, A.M., Arkin, A.P., and Stahl, D.A. (2014) The energy-conserving electron transfer system used by Desulfovibrio alaskensis strain G20 during pyruvate fermentation involves reduction of endogenously formed fumarate and cytoplasmic and membrane-bound complexes, Hdr-Flox and Rnf. *Environ Microbiol* 16: 3463–3486.
- Neidhardt, F. (1987). Chemical Composition of Escherichia coli and Salmonella typhimurium: Cellular and Molecular Biology. Washington, DC: American Society for Microbiology.
- Odom, J.M, and Peck, H.D. (1981) Hydrogen cycling as a general mechanism for energy coupling in the sulfate-reducing bacteria, Desulfovibrio sp. *FEMS Microbiol Lett* **12**: 47–50.
- Pereira, I.A.C., Ramos, A.R., Grein, F., Marques, M.C., Silva, D., Marques, S., and Venceslau, S.S. (2011) A comparative genomic analysis of energy metabolism in sulfate reducing bacteria and archaea. *Front Microbiol* **2**: 69.
- Pereira, P.M., He, Q., Valente, F.M.A., Xavier, A.V., Zhou, J., Pereira, I.A.C., and Louro, R.O. (2008) Energy metabolism in Desulfovibrio vulgaris Hildenborough: insights from transcriptome analysis. *Antonie Van Leeuwenhoek* 93: 347–362.
- Price, M.N., Deutschbauer, A.M., Kuehl, J.V., Liu, H., Witkowska, H.E., and Arkin, A.P. (2011) Evidence-based annotation of transcripts and proteins in the sulfate-reducing bacterium Desulfovibrio vulgaris Hildenborough. *J Bacteriol* **193**: 5716–5727.
- Price, M.N., Ray, J., Wetmore, K.M., Kuehl, J.V., Bauer, S., Deutschbauer, A.M., and Arkin, A.P. (2014) The genetic basis of energy conservation in the sulfate-reducing bacterium Desulfovibrio alaskensis G20. Frontiers of Microbiology 31 Oct 2014.

- Ramos, A.R., Grein, F., Oliveira, G.P., Venceslau, S.S., Keller, K.L., Wall, J.D., and Pereira, I.A.C. (2015) The FlxABCD-HdrABC proteins correspond to a novel NADH dehydrogenase/heterodisulfide reductase widespread in anaerobic bacteria and involved in ethanol metabolism in Desulfovibrio vulgaris Hildenborough. *Environ Microbiol* 17: 2288–2305.
- Ramos, A.R., Keller, K.L., Wall, J.D., and Pereira, I.A.C. (2012) The membrane QmoABC complex interacts directly with the dissimilatory Adenosine 5'-phosphosulfate reductase in sulfate reducing bacteria. *Front Microbiol* **3**: 137.
- Santos, A.A., Venceslau, S.S., Grein, F., Leavitt, W.D., Dahl, C., Johnston, D.T., and Pereira, I.A.C. (2015) A protein trisulfide couples dissimilatory sulfate reduction to energy conservation. *Science* 350: 1541–1545.
- Schellenberger, J., Park, J.O., Conrad, T.M., and Palsson, B.Ø. (2010) BiGG: a biochemical genetic and genomic knowledgebase of large scale metabolic reconstructions. *BMC Bioinformatics* **11**: 213.
- Schellenberger, J., Lewis, N.E., and Palsson, B.Ø. (2011a) Elimination of thermodynamically infeasible loops in steady-state metabolic models. *Biophys J* **100**: 544–553.
- Schellenberger, J., Que, R., Fleming, R.M.T., Thiele, I., Orth, J.D., Feist, A.M., *et al.* (2011b) Quantitative prediction of cellular metabolism with constraint-based models: the COBRA Toolbox v2.0. *Nat Protoc* **6**: 1290–1307.
- Stolyar, S., Van Dien, S., Hillesland, K.L., Pinel, N., Lie, T.J., Leigh, J.A., and Stahl, D.A. (2007) Metabolic modeling of a mutualistic microbial community. *Mol Syst Biol* **3**: 92.
- Traore, A.S., Gaudin, C., Hatchikian, C.E., Gall, J.L., and Belaich, J.P. (1983) Energetics of growth of a defined mixed culture of Desulfovibrio vulgaris and Methanosarcina barkeri: maintenance energy coefficient of the

- sulfate-reducing organism in the absence and presence of its partner. *J Bacteriol* **155**: 1260–1264.
- Venceslau, S.S., Lino, R.R., and Pereira, I.A.C. (2010) The
 - Qrc membrane complex, related to the alternative Complex III, is a menaquinone reductase involved in sulfate respiration. *J Biol Chem* **285**: 22774–22783.
- Villanueva, L., Haveman, S.A., Summers, Z.M., and Lovley, D.R. (2008) Quantification of Desulfovibrio vulgaris dissimilatory sulfite reductase gene expression during electron donor- and electron acceptor-limited growth. *Appl Environ Microbiol* **74**: 5850–5853.
- Vita, N., Valette, O., Brasseur, G., Lignon, S., Denis, Y., Ansaldi, M., et al. (2015) The primary pathway for lactate oxidation in Desulfovibrio vulgaris. Front Microbiol 6: 606.
- Voordouw, G. (1995) The genus Desulfovibrio: the centennial. *Appl Environ Microbiol* **61**: 2813–2819.
- Walker, C.B., He, Z., Yang, Z.K., Ringbauer, J.A., He, Q., Zhou, J., et al. (2009) The electron transfer system of syntrophically grown Desulfovibrio vulgaris. J Bacteriol 191: 5793–5801.

Supporting Information

Additional Supporting Information may be found in the online version of this article at the publisher's web-site:

Table S1. Model media formulation.

- **Table S2.** Predicted growth rate, NGAM, GAM and key metabolic ratio for model variants under four tested growth conditions.
- **Table S3.** Predicted FVA results for key electron transfer reactions for iJF744 under the four tested growth conditions.
- Table S4. Results from essential reaction analysis.